POLITECNICO DI TORINO
Repository ISTITUZIONALE

Brittle crack deflection: Phase Field vs Theory of Critical Distances

Original
Brittle crack deflection: Phase Field vs Theory of Critical Distances / Petraglia, G., Cornetti, P., Grillo, A., Sapora, A.. - In: ZEITSCHRIFT FUR ANGEWANDTE MATHEMATIK UND PHYSIK. - ISSN 0044-2275. - ELETTRONICO. - 77:2(2026), pp. 1-19. [10.1007/s00033-025-02697-2]

Availability:
This version is available at: 11583/3006530 since: 2026-01-13T16:06:40Z

Publisher:
Springer Nature

Published
DOI:10.1007/s00033-025-02697-2

Terms of use:

This article is made available under terms and conditions as specified in the corresponding bibliographic description in the repository

Publisher copyright

(Article begins on next page)

27 November 2026

Brittle crack deflection: Phase Field vs Theory of Critical Distances

Giacomo Petraglia, Pietro Cornetti, Alfio Grillo and Alberto Sapora

Abstract. Depending on material properties and geometrical features, cracks in pre-cracked structures can propagate collinearly or kink, eventually following a curved path. Several approaches have been proposed in the literature to study this behaviour, with different complexity depending on the number of involved parameters. The novelty of this study lies in the use of a Phase Field model to predict crack paths in brittle cracked geometries under Mode-I loading conditions. The approach is based on a quasi-static analysis to describe the elastic phase of the tensile test, followed by the simulation of crack initiation and propagation in order to predict the full crack path. Numerical outcomes are compared with experimental results reported in the literature: the model provides accurate predictions for critical loads and crack paths. Results by the Point Method and Line Method in the framework of the Theory of Critical Distances are also provided to test the consistency of the proposed approach.

Mathematics Subject Classification (2010). 74A45, 49J40.

Keywords. Fracture mechanics, Phase Field model, Variational formulation, Crack path, Crack kinking, Theory of Critical Distances.

1. Introduction

Cracked brittle specimens represent one of the most widely adopted benchmark configurations in fracture mechanics, providing an ideal framework for both experimental investigation and numerical modeling of crack propagation. In such configurations, deviations from straight crack paths and reductions in fracture strength are commonly observed (even under pure Mode-I loading conditions [4]) thereby highlighting the need for a refined description of the stress field in the neighborhood of the crack tip. Classical stress intensity factors (SIFs) quantify the singular component of this field at the notch tip, whereas higher-order terms in Williams' asymptotic expansion govern its distribution at certain distances from the crack tip. The first non-singular term in the expansion, the so-called T-stress, represents a constant stress parallel to the crack plane and has been identified as a key parameter in crack path prediction. To assess its influence, several criteria have been proposed based on stress [24, 58, 13], energy [7], or combined approaches [35].

The effect of the T-stress sign on crack path stability under pure Mode-I loading has long been debated. Using a first-order perturbation of complex potentials, Cotterell and Rice [20] concluded that negative T-stress promotes stable propagation, whereas positive T-stress induces instability — a result consistent with earlier findings [5]. However, subsequent experiments revealed the existence of a positive threshold [48, 14], beyond which unstable crack growth occurs, challenging the idea that stability depends solely on the T-stress sign. Methods to estimate the T-stress threshold include the coupled criterion [35] and Finite Fracture Mechanics [19, 46]. Regarding Theory of Critical Distances (TCD) implementations, Smith et al. [51] and Sapora et al. [45] proposed a Point Method (PM) and a

This preprint has not undergone peer review or any post-submission improvements or corrections. The Version of Record of this article is published in *Zeitschrift für angewandte Mathematik und Physik*, and is available online at https://doi.org/10.1007/s00033-025-02697-2

Line Method (LM), respectively, taking into account T-stress effects. In particular, Sapora et al. [45] applied the TCD implementing a curved crack advance, showing the presence of a critical T-stress value beyond which curved crack propagation is favored, since it leads to a lower fracture load than that associated with straight crack propagation.

While TCD offers valuable predictions for crack propagation loads and kinking angles, its applicability becomes limited when the goal is to predict the entire trajectory of the crack, due to its local nature and lack of a mechanism for incremental crack propagation. For this purpose, the Phase Field (PF) model emerges as a powerful alternative. Rooted in variational principles, the PF model regularizes Griffith's theory via Γ-convergence [11], and allows for a continuous description of fracture evolution without prescribing the crack path *a priori*.

Thanks to its variational formulation and diffuse interface representation, the PF model has been successfully employed to capture crack nucleation and growth in a wide variety of settings, including heterogeneous composites [41, 36], ductile matrices [32, 1], and fatigue scenarios [29, 27]. Its ability to naturally account for complex crack topologies—including initiation, deflection, branching, and merging—makes it particularly attractive for simulating cracked geometries under diverse loading conditions. Previous studies have shown good agreement between PF predictions and experimental results for mixed-mode loading and dynamic propagation [31, 30, 42, 44].

Despite the extensive literature on PF applications, to the best of the authors' knowledge, no prior studies have explicitly addressed the prediction of curved crack trajectories in cracked brittle specimens subjected to pure Mode-I loading. In this work, we explore this scenario through numerical simulations carried out within the FEniCSx computational framework [6], focusing on five cracked poly-methyl methacrylate (PMMA) specimens experimentally tested by Ayatollahi et al. [4]. Finally, PF results are compared against predictions obtained from PM and LM formulations.

2. Experimental data

Given the importance of the experimental dataset for validating the proposed approach, in this section we provide a brief summary of the experiments conducted by Ayatollahi et al. [4]. The dataset consisted of five different geometries for the fracture tests: the Compact Tension (CT), two variants of the Double Cantilever Beam (DCB), and two variants of the Tapered Double Cantilever Beam (TDCB). For each geometry, three identical specimens were tested. Tests were carried out under pure Mode-I loading conditions and (quasi-)static displacement control with a rate $U_{\text{imp}} = 0.1$ mm/min. An advantage of selecting these specific specimen types was that, despite their simple shapes, they enabled the generation of different crack paths associated with varying T-stress levels. Figs. 1, 2 and 3 show the considered geometries. The dimensions of the specimens are listed in Table 1.

Specimen	W **[mm]**	h **[mm]**	a **[mm]**	τ
CT	30	30	15	0.06
DCB1	90	30	45	0.22
DCB2	150	30	75	0.25
TDCB1	90	$h_1 = 30$, $h_2 = 90$	45	0.10
TDCB2	150	$h_1 = 30$, $h_2 = 90$	75	0.24

TABLE 1. Geometrical parameters and corresponding dimensionless T-stresses τ for the tested specimens [4]. W is the specimen width, h is the height, and a is the initial crack length. For TDCB specimens, h_1 and h_2 denote the two different heights in Fig. 1 and 3. For all specimens, $t = 10$ mm.

2.1. Material properties

All specimens were made of PMMA. The elastic modulus $E = 2.9$ GPa and the tensile strength $\sigma_u = 55$ MPa were experimentally determined in [4] through tensile tests conducted according to

This preprint has not undergone peer review or any post-submission improvements or corrections. The Version of Record of this article is published in *Zeitschrift für angewandte Mathematik und Physik*, and is available online at https://doi.org/10.1007/s00033-025-02697-2

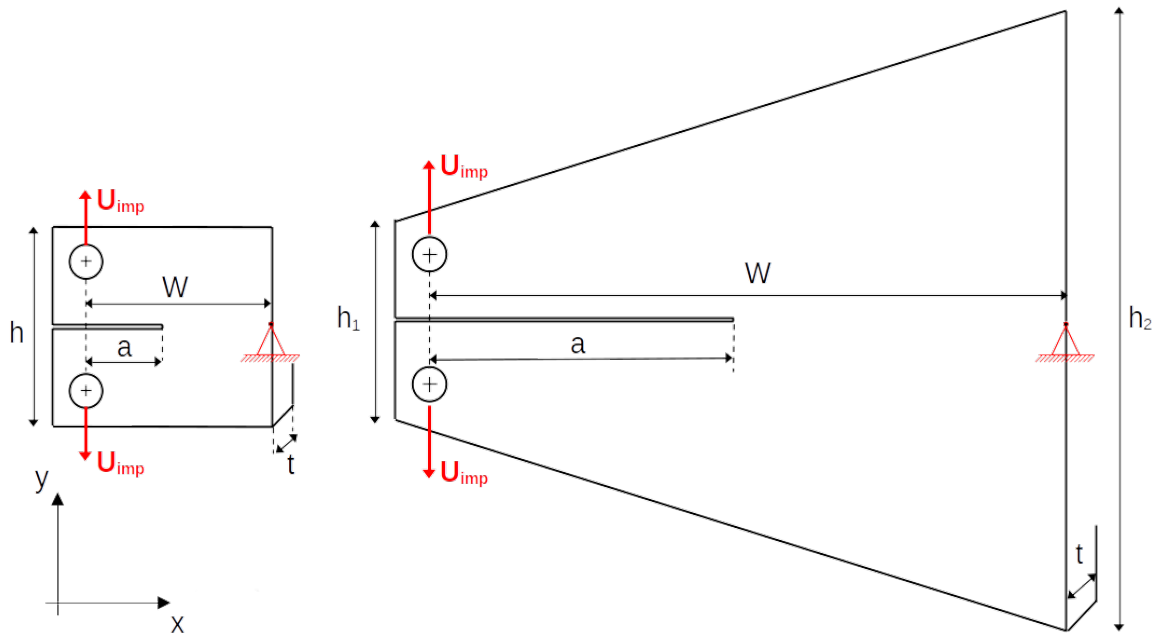

FIGURE 1. CT and TDCB1 geometries

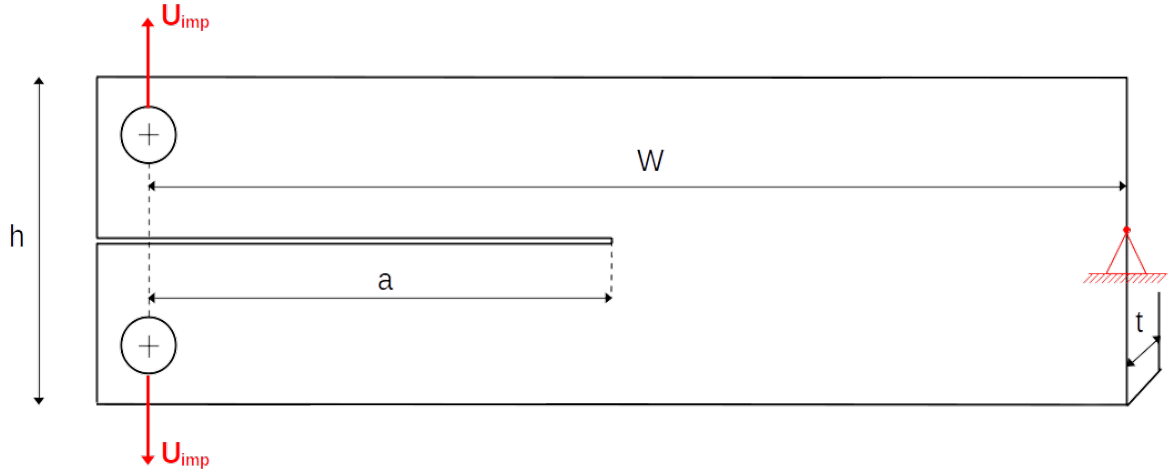

FIGURE 2. DCB geometry

the ASTM D638 standard. Poisson's ratio ν was assumed to be 0.35, as reported in [3]. The Mode-I SIFs K_{I} and the T-stresses related to the examined geometries were evaluated in [4] via an interaction integral method built in FE software [52]. T-stresses were adimensionalized by means of the expression [19]:

$$\tau = \frac{T\sqrt{r_c}}{K_{\mathrm{I}}} \tag{1a}$$

with

$$r_c = \frac{1}{2\pi}\left(\frac{K_{\mathrm{IC}}}{\sigma_u}\right)^2 \tag{1b}$$

This preprint has not undergone peer review or any post-submission improvements or corrections. The Version of Record of this article is published in *Zeitschrift für angewandte Mathematik und Physik*, and is available online at https://doi.org/10.1007/s00033-025-02697-2

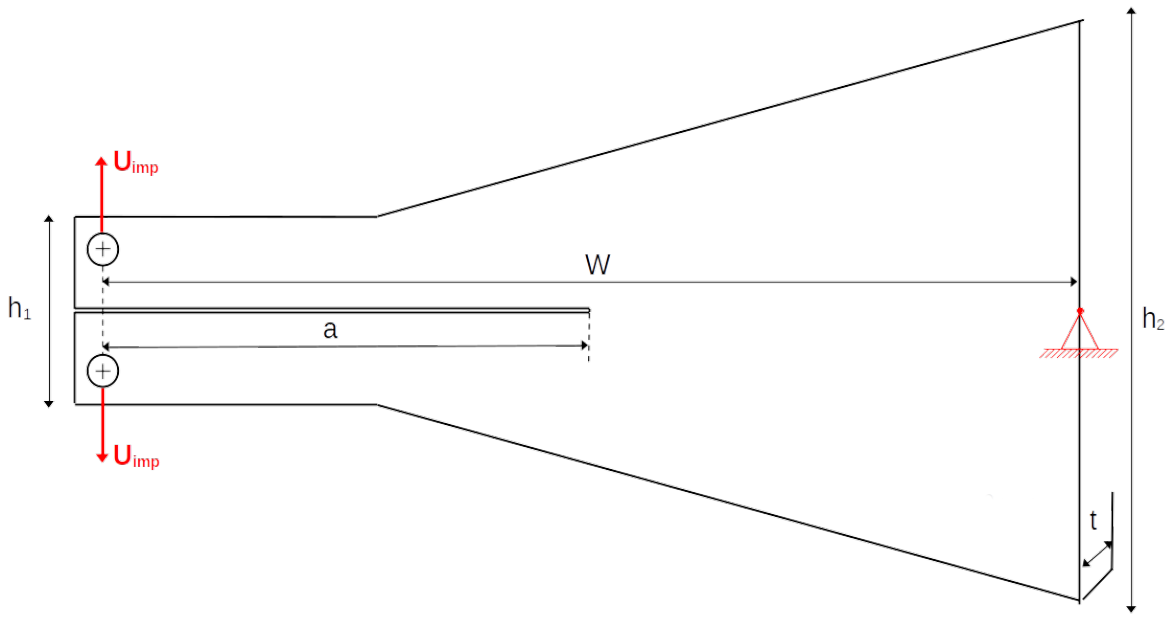

FIGURE 3. TDCB2 geometry

where r_c is the PM characteristic distance (see Sect. 3.2). Table 1 lists τ values reported in [4]. Dimensionless T-stresses depend on material properties (through K_{IC} and σ_u) and on geometrical features (through the crack length-to-width ratio a/W) [61].

The value of K_{IC} for PMMA was defined in [4] as the SIF for the CT geometry at incipient failure, obtaining $K_{\mathrm{IC}} \approx 1.402$ MPa$\sqrt{\mathrm{m}}$. This choice was justified by the fact that, due to their geometrical properties, CT specimens exhibit a negligible T-stress contribution [2]. Hence, under such conditions, the specimen response can be described within the framework of LEFM and the material fracture toughness can be approximated by the critical Mode-I SIF ($K_{\mathrm{If}}^{\mathrm{CT}} \approx K_{\mathrm{IC}}$). The value of the critical energy release rate G_c is determined by applying the well-known Irwin's law, considered here under plane strain conditions:

$$G_c = \frac{K_{\mathrm{IC}}^2 \left(1-\nu^2\right)}{E} = 0.593 \text{ MPa mm} \tag{2}$$

Given the relatively large thickness of the specimens ($t = 10$ mm) compared to their in-plane dimensions (see Table 1), plane strain conditions are considered appropriate and adopted for all numerical simulations.

3. Methodological framework

This section presents the methodological framework adopted in the present study to model brittle fracture, detailing the numerical approaches employed: PF model and TCD.

3.1. Phase Field (PF) model

The PF model applied to brittle fracture formulates the quasi-static evolution problem as a minimization condition on the following energy functional:

$$\mathcal{E}_{tot}\left(\mathbf{u},\alpha\right) = \mathcal{E}_S\left(\mathbf{u},\alpha\right) + \mathcal{E}_F\left(\alpha,\nabla\alpha\right) \tag{3}$$

The expression for the total energy $\mathcal{E}_{tot}$ is given by the sum of the strain energy $\mathcal{E}_S$, which quantifies the energy stored in the system due to elastic deformation, and the fracture energy $\mathcal{E}_F$, which accounts for the energy expended during fracture processes. The scalar field $\alpha\left(\mathbf{x}\right) \in [0,1]$ quantifies the damage

This preprint has not undergone peer review or any post-submission improvements or corrections. The Version of Record of this article is published in *Zeitschrift für angewandte Mathematik und Physik*, and is available online at https://doi.org/10.1007/s00033-025-02697-2

state of the material. Accordingly, $\alpha = 0$ corresponds to an intact material, $0 < \alpha < 1$ denotes partial damage and $\alpha = 1$ represents complete failure. Additionally, the damage rate α is subject to an irreversibility condition, thereby preventing the occurrence of self-healing effects in the material.
Due to the PF model's inclusion in the class of Gradient Damage Models [42], the general form of the fracture energy functional $\mathcal{E}_F$ can be expressed as:

$$\mathcal{E}_F(\alpha, \nabla\alpha) = \frac{G_c}{c_w} \int_\Omega \left(\frac{w(\alpha)}{\ell} + \ell \, \nabla\alpha \cdot \nabla\alpha \right) \, \mathrm{d}\mathbf{x} \tag{4}$$

The function $w(\alpha)$ denotes the normalized energy dissipation density of the material in the case of a homogeneous damage process (i.e. $\nabla\alpha = 0$). Furthermore, c_w is a dimensionless scaling parameter that enforces the specific energy expended during the fracture of a uniaxial tensile bar to match the critical energy release rate G_c. The parameter ℓ defines the internal length, governing the size of the transition zone between the damaged and intact material. The expression for $\mathcal{E}_F$ highlights the role of ℓ in balancing the local and gradient (non-local) components of the energy. As ℓ increases, the gradient term becomes more dominant, promoting a smoother transition of α due to its regularizing effect. Interestingly, the physical significance of ℓ can be elucidated by drawing a comparison between the variational approach and the coupled criterion [34]: in this context, and from the perspective of Finite Fracture Mechanics, ℓ emerges as an intermediate scale between the Irwin's material length and the size of the instantaneous crack initiation zone [39].

Regarding the strain energy term $\mathcal{E}_S$:

$$\mathcal{E}_S(\mathbf{u}, \alpha) = \int_\Omega g(\alpha) \;\; \psi(\varepsilon(\mathbf{u})) \, \mathrm{d}\mathbf{x}, \tag{5a}$$

$$g(\alpha) = (1 - \alpha)^2, \tag{5b}$$

$$\psi(\varepsilon(\mathbf{u})) = \frac{\lambda}{2} \left[\mathrm{tr} \, \varepsilon(\mathbf{u}) \right]^2 + \mu \, \varepsilon(\mathbf{u}) : \varepsilon(\mathbf{u}) \tag{5c}$$

The expression for $g(\alpha)$ defines the degradation function: it governs how the influence of strain energy $\mathcal{E}_S$ evolves as α increases. Independently of its application on the standard $\mathcal{E}_S$ expression, its effect must guarantee a monotonic decrease in $\mathcal{E}_S$ as α increases. The expression for the classic strain energy density ψ (where λ and μ are the Lamé coefficients and $\varepsilon(\mathbf{u})$ is the linear strain tensor) serves as the basis for the No-Split energetic formulation [17], in which all components of the deformation are equally influenced by the damage evolution. The use of an energetic decomposition strategy (with the most popular formulations of which having been extensively reviewed in [22]) was not considered necessary, since no compressive stress states were expected to occur in the most critically loaded areas of the investigated geometries. Considering the adopted material properties (Sect. 2.1) and the use of the PF model in the No-Split formulation, the characteristic length ℓ is computed using the following expression [17]:

$$\ell = \frac{3 G_c E}{8 \sigma_u^2 (1 - \nu^2)} = 0.243 \text{ mm} \tag{6}$$

To further refine the model definition, the following expression is introduced [22]:

$$w(\alpha) = \alpha \tag{7}$$

The definition of the local energy density $w(\alpha)$ characterizes the AT1 damage law, which represents one of the most widely adopted choices for damage constitutive functions. In contrast to other commonly used damage laws (such as AT2, for which $w(\alpha) = \alpha^2$), it provides the advantage of describing a purely elastic material response under relatively low loads, making the model more consistent with actual material behavior [9].

This preprint has not undergone peer review or any post-submission improvements or corrections. The Version of Record of this article is published in *Zeitschrift für angewandte Mathematik und Physik*, and is available online at https://doi.org/10.1007/s00033-025-02697-2

3.2. Theory of Critical Distances: Point Method (PM) approach

According to PM [55, 57, 53] and with reference to the coordinate system illustrated in Fig. 4a, failure occurs when the circumferential stress $\sigma_{\theta\theta}$ is equal to the ultimate tensile strength σ_u at a given distance r_c (Eq. (1b)) from the crack tip, along a direction forming an angle θ_c with the crack plane:

$$\sigma_{\theta\theta}\left(r = r_c,\ \theta = \theta_c\right) = \sigma_u \tag{8}$$

It is worth emphasizing that the critical distance r_c depends exclusively on material properties, in contrast to approaches like Finite Fracture Mechanics [34, 18], where the finite crack advance also depends on geometrical features, thus becoming a structural parameter [45]. Taking T-stress effects into account [49, 51], the expression of the circumferential stress field $\sigma_{\theta\theta}$ in the proximity of the pre-existing crack tip of length a in polar coordinates (with $r \ll a$) can be expressed as:

$$\sigma_{\theta\theta}\left(r, \theta\right) = \frac{K_{\mathrm{I}}}{\sqrt{2\pi r}} f^{I}_{\theta\theta}\left(\theta\right) + T \sin^2\theta \tag{9}$$

where K_{I} is the Mode-I SIF related to the pre-existing crack and $f^{I}_{\theta\theta}\left(\theta\right) = \frac{1}{4}\left[3\cos\left(\theta/2\right) + \cos\left(3\theta/2\right)\right]$ is the correlated angular function [59]. The last summand of Eq. (9) represents the T-stress contribution, i.e. the first non-singular term in the stress field expansion.

At this point, substituting Eq. (9) into Eq. (8) yields:

$$\frac{K_{\mathrm{I}}}{\sqrt{2\pi r_c}} f^{I}_{\theta\theta}\left(\theta\right) + T \sin^2\theta = \sigma_u \tag{10}$$

with θ acting as a parameter. Recalling the expression of the characteristic distance r_c in Eq. (1b) and considering the dimensionless T-stress τ as defined in Eq. (1a), at incipient failure ($K_{\mathrm{I}} = K_{\mathrm{If}}$), the following condition must be fulfilled:

$$\frac{K_{\mathrm{If}}}{K_{\mathrm{IC}}} = \frac{1}{f^{I}_{\theta\theta}\left(\theta\right) \ + \ \sqrt{2\pi}\tau \sin^2\theta} \tag{11}$$

The critical Mode-I SIF K_{If} corresponds to the critical angle θ_c, defined as the value of the angular parameter θ within the interval $[0, \pi/2]$ that maximizes the denominator of Eq. (11). It is worth noting that the problem can be solved once the structural properties and loading conditions of the mechanical setup are known, allowing the determination of the expression for τ.

Within this framework it is possible to assume that the crack propagates along a curved path, as showed in Fig. 4b. As proposed in [33], the crack advance can be described as:

$$\Gamma(m) = (m, bm^{\frac{3}{2}}), \tag{12}$$

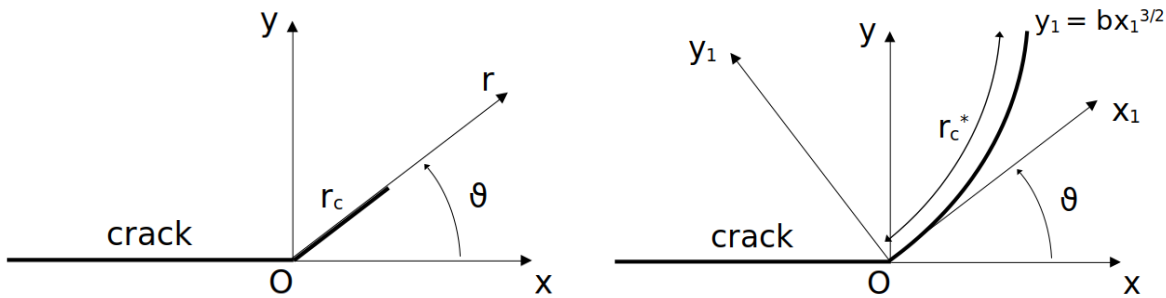

(A) Straight crack advance.

(B) Curved crack advance.

FIGURE 4. Reference frames for a cracked element. The angular variable is denoted by θ, with its critical value θ_c being the angle that minimizes the adopted failure condition

This preprint has not undergone peer review or any post-submission improvements or corrections. The Version of Record of this article is published in *Zeitschrift für angewandte Mathematik und Physik*, and is available online at https://doi.org/10.1007/s00033-025-02697-2

where b is the curvature parameter. The shape $\sim m^{\frac{3}{2}}$ ensures compatibility between the crack path geometry and the asymptotic expansion of the stress field near the tip, making the application of the Principle of Local Symmetry (PLS) consistent [26]: according to the PLS, the crack propagates in a direction such that the Mode-II stress intensity factor at the crack tip vanishes. In this context, Leblond [33] derived an expansion of the crack path by imposing this condition, showing that the first non-trivial term of the series must scale as $m^{3/2}$. Moreover, b constitutes an additional variable for the PM formulation, and its values are obtained from the conducted numerical analyses as a function of τ. With this assumption, the PM failure criterion (Eq. (8)) can be expressed as:

$$\sigma_{\theta\theta}\left(r(m)=r_c^*,\ \theta(m)=\theta_c^*\right)=\sigma_u, \tag{13}$$

Thus, the curved PM failure criterion states that, at incipient failure ($K_{\mathrm{I}}=K_{\mathrm{If}}$), the condition expressed by Eq. (10) has to be fulfilled, with the difference that r_c is replaced with r_c^*:

$$r_c^*=r(m_c)=\sqrt{x^2(m_c)+y^2(m_c)}=\sqrt{m_c^2+b^2m_c^3}, \tag{14a}$$

where

$$m_c=\frac{4}{9b^2}\left[\left(\frac{27}{8}b^2r_c+1\right)^{\frac{2}{3}}-1\right] \tag{14b}$$

The quantity r_c^* denotes the PM critical distance obtained by reaching a length $l=r_c$ along the curved crack described by the parametric curve Γ, and m_c denotes the critical curvilinear coordinate obtained imposing $\int_0^{m_c}\|\Gamma'(m)\|\ \mathrm{d}m=r_c$ (i.e., by imposing that the length of the curve, evaluated at the critical value m_c of the parameter, equals the critical length r_c). Substituting Eq. (14b) into Eq. (14a) yields:

$$r_c^*=\frac{1}{9}\Bigg(81r_c^2+\frac{r_c\left(48-9\left(8+27b^2r_c\right)^{1/3}\right)}{b^2} +\frac{8\left(-6+\left(8+27b^2r_c\right)^{1/3}+\left(8+27b^2r_c\right)^{2/3}\right)}{3b^4}\Bigg)^{1/2} \tag{15}$$

The new expression for curved crack paths has to be solved by varying both the curvature parameter b and the angular coordinate θ over the interval $[0,\pi/2]$. For every τ, the critical values θ_c and b_c correspond to the pair of values that minimizes K_{If} in the expression of the PM curved failure criterion.

3.3. Theory of Critical Distances: Line Method (LM) approach

According to LM [56, 40] for straight crack propagation (see Fig. 4a), failure occurs when the average circumferential stress of $\sigma_{\theta\theta}$, computed over a characteristic distance $r_{c,\mathrm{LM}}$, reaches the ultimate tensile strength σ_u:

$$\frac{1}{r_{c,\mathrm{LM}}}\int_0^{r_{c,\mathrm{LM}}}\sigma_{\theta\theta}\left(r,\theta\right)\ \mathrm{d}r=\sigma_u, \tag{16a}$$

where

$$r_{c,\mathrm{LM}}=\frac{2}{\pi}\left(\frac{K_{\mathrm{IC}}}{\sigma_u}\right)^2 \tag{16b}$$

Taking into account the stress field expansion (Eq. (9)) and supposing a curved crack propagation described by the parametric curve reported in Eq. (12), the average stress failure condition is thus recast in the following form [45]:

$$\frac{1}{r_{c,\mathrm{LM}}}\int_\Gamma\sigma_{\theta\theta}\,ds=\frac{1}{r_{c,\mathrm{LM}}}\int_0^{m_{c,\mathrm{LM}}}\sigma_{\theta\theta}(r(t),\theta(t))\sqrt{1+\frac{9}{4}b^2t}\,dt=\sigma_u, \tag{17}$$

where

$$m_{c,\mathrm{LM}}=\frac{4}{9b^2}\left[\left(\frac{27}{8}b^2r_{c,\mathrm{LM}}+1\right)^{\frac{2}{3}}-1\right] \tag{18}$$

This preprint has not undergone peer review or any post-submission improvements or corrections. The Version of Record of this article is published in *Zeitschrift für angewandte Mathematik und Physik*, and is available online at https://doi.org/10.1007/s00033-025-02697-2

It is worth noting that the expressions for r_c (Eq. (1b)) and $r_{c,\mathrm{LM}}$ (Eq. (16b)) are not arbitrary. Their specific forms are required to ensure that $K_\mathrm{I} = K_\mathrm{IC}$, as expected from LEFM in the case of a large cracked geometry [47].

4. Numerical setup

In this study, the adopted PF model was developed within the open-source finite element framework FEniCSx [6]. The implementation was carried out in the spirit of the coding style and structure proposed in [15]. All meshes were generated using the open-source software Gmsh [25], which served to define both the geometries and the corresponding spatial discretizations. Fig. 5 shows an example of the meshing strategy adopted for a DCB geometry. A refined mesh can be observed near the crack tip, where a higher resolution is required, while the mesh becomes progressively coarser at increasing distances. To prevent preferential crack paths induced by locally refined regions, an unstructured mesh with uniform element size of approximately $\delta = \ell/5$ was imposed in the area immediately ahead of the crack tip. As stated in [16], no adaptive mesh refinement was employed to prevent wave reflections due to the relatively higher stiffness of the coarser elements. Moreover, although adaptive mesh refinement could potentially reduce the overall computational cost, it may introduce artificial stiffness contrasts that can act as unintended barriers or guides for crack propagation, thereby compromising the physical reliability of the conducted simulations. With regard to the implementation of the boundary conditions, the displacement rate U_imp was applied to the nodes located at the outermost edges of the pins (see Fig. 5), in accordance with the procedure proposed by [42].

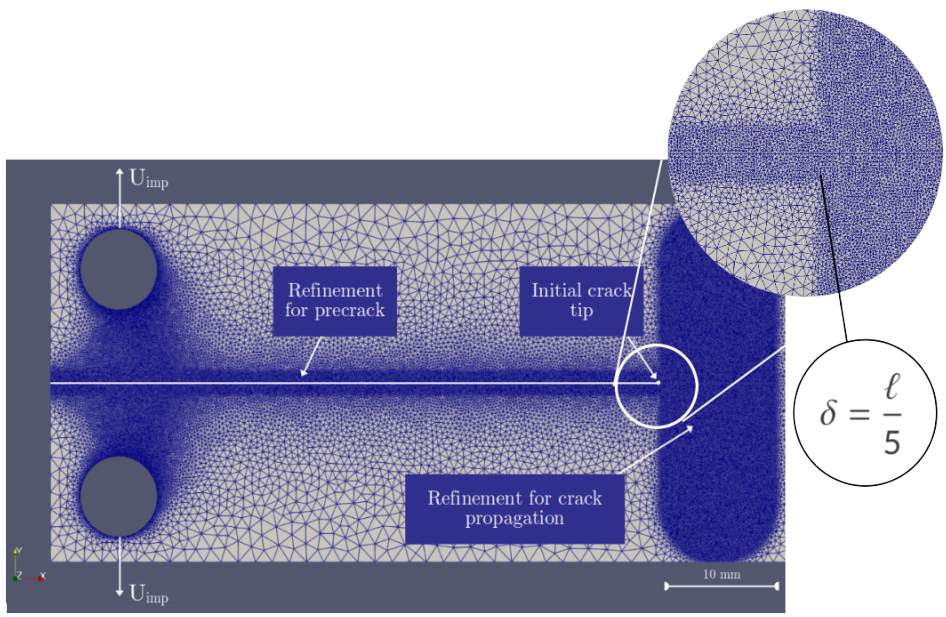

FIGURE 5. A mesh detail for the DCB1 geometry. The mesh element size δ is set to $\ell/5$ (where ℓ is given by Eq. (6)) in the vicinity of the pre-crack and in the region ahead of the initial crack tip

4.1. Criterion for crack nucleation

The threshold reaction force on loading pins, that defines the critical load, is numerically estimated for each geometry. This load corresponds to the onset of damage nucleation: a suitable criterion must be defined within the PF framework to identify this transition. In this context, the condition for crack initiation is identified as the point at which the crack tip, initially located at the origin of the

This preprint has not undergone peer review or any post-submission improvements or corrections. The Version of Record of this article is published in *Zeitschrift für angewandte Mathematik und Physik*, and is available online at https://doi.org/10.1007/s00033-025-02697-2

reference system, begins to move in response to the evolving damage field [37]. For this purpose, Crack Tip Tracking Algorithms (CTTA, [28]) become essential for analyzing the crack tip kinematics. They operate by evaluating the variable α at a fixed distance d_{CTTA} ahead of the current crack tip. The algorithm provides crack tip advancement when $\alpha \geq \alpha_{\mathrm{CTTA}}$ at a radial distance from the current crack tip $r = d_{\mathrm{CTTA}}$, where α_{CTTA} is a fixed threshold value. In the literature several choices for d_{CTTA} and α_{CTTA} have been proposed, primarily based on experimental validation studies of PF models for predicting critical loads [30, 10, 28, 54].

Following the methodology outlined in [43], this study sets:

$$\begin{cases} d_{\mathrm{CTTA}} = \ell \\ \alpha_{\mathrm{CTTA}} = 0.25 \end{cases} \tag{19}$$

Hence, critical load values are identified as the reaction forces measured on the pins when α first reaches the threshold α_{CTTA} at a position located one PF characteristic length ahead of the initial crack tip.

4.2. Definition of the pre-existing crack

Another critical aspect concerns the definition of the pre-existing crack in the numerical domain. The most intuitive strategy consists in explicitly introducing the pre-existing crack through the mesh (mentioned as '*Mesh induced initial crack*' in [60]). On the other hand, numerous studies have reported that such an approach may lead to a significant overestimation of the critical loads [31, 30, 50]. In the present work, following the approach referred to as the '*PF induced initial crack*' [28], the pre-crack is introduced within the PF numerical framework by prescribing Dirichlet boundary conditions ($\alpha = 1$) at the nodes lying along the extension of the initial crack. Within our scope of investigation, which involves structures characterized by the presence of pre-existing cracks, the PF induced initial crack definition proves particularly reliable [54]. It is worth noting that the model is indeed capable of accurately predicting crack nucleation in the presence of different types of defects, such as notches or holes [16]. However, the reliability of results obtained using the same pre-crack definition may differ from scenario to scenario [31].

4.3. Numerical evaluation of critical Stress Intensity Factors (SIFs)

One of the goals of this study is to assess the dependence of fracture strength on the geometry-induced T-stress [4, 45, 19] through PF numerical analysis. To evaluate the critical SIF for the examined geometries, Irwin's relation is employed under the assumption of pure Mode-I loading conditions and plane strain conditions:

$$K_{\mathrm{If}} = \sqrt{\frac{G_{\mathrm{f}} E}{1-\nu^2}} \tag{20}$$

G_{f} denotes the energy release rate at failure, i.e. G evaluated at the time when the crack nucleation condition (Sect. 4.1) is first satisfied. The energy release rate was evaluated using the G-θ method [23], a rigorous approach that starting from the classical definition $G = -\frac{d\mathcal{E}}{da}$ (where a denotes the crack length), introduces a virtual crack extension δl, expresses the total energy as a function of l, and computes its derivative [21]:

$$G = -\left.\frac{d\mathcal{E}_l}{dl}\right|_{l=0} \tag{21}$$

5. Results and discussion

In this section, PF outcomes are compared with experimental results reported in [4] and theoretical predictions provided by TCD approaches.

This preprint has not undergone peer review or any post-submission improvements or corrections. The Version of Record of this article is published in *Zeitschrift für angewandte Mathematik und Physik*, and is available online at https://doi.org/10.1007/s00033-025-02697-2

Geometry	Reference values	PF	Relative error (%)
TDCB1	36.7	36.0	1.91
CT	25.3	22.9	9.49
TDCB2	17.5	18.4	5.43
DCB1	14.1	13.5	4.25
DCB2	8.70	8.77	0.80

TABLE 2. Critical loads per unit thickness [N/mm]. Reference values are based on the experimental results reported in [4], except for the CT geometry, for which the value is derived from the relation provided in [12].

5.1. Critical load predictions

The post-processing phase employs the virtual work principle-based approach described in [8] to evaluate the resulting reaction forces on the pin boundaries. Table 2 reports the critical load predictions per unit thickness obtained through the PF simulations, compared with the reference results. The last column shows the relative error.

PF predictions show good agreement with the reference data across all geometries, with relative errors all below 10%. It is worth noting that the prediction for the CT specimen was compared to the expected critical load rather than to the experimental result from [4], using the following relation between the applied load P and the Mode-I SIF for CT geometries [12]:

$$P\left(K_{\mathrm{I}},\, a,\, W\right) = K_{\mathrm{I}} \sqrt{\frac{W}{\pi}} \left[16.7 \left(\frac{a}{W}\right)^{1/2} - 104.7 \left(\frac{a}{W}\right)^{3/2} + 369.9 \left(\frac{a}{W}\right)^{5/2} - 573.8 \left(\frac{a}{W}\right)^{7/2} + 360.5 \left(\frac{a}{W}\right)^{9/2} \right]^{-1} \tag{22}$$

Hence, for the considered CT geometry (for $K_{\mathrm{I}} = K_{\mathrm{IC}} = 1.402$ MPa$\sqrt{\mathrm{m}}$) we have an expected critical load $P_C = 25.3$ N/mm (Table 2). Overall, the results confirm the reliability of the adopted model in characterizing fracture behavior across the investigated geometrical configurations. While the comparison for the CT specimen is not directly based on experimental data, it is nonetheless well founded, as it relies on a consolidated analytical relation and on the literature-validated value of K_{IC} [4]. Therefore, this discrepancy does not undermine the validity of the analyses conducted on the other geometries, whose predictions exhibit excellent agreement with experimental results in terms of critical load.

5.2. Crack path predictions

In this subsection, a qualitative analysis of the fracture path predicted by the PF model is carried out. The crack trajectory is determined based on the distribution of the damage field α. The propagation direction, possible deviations, and the agreement with experimental evidence are discussed.

5.2.1. CT and TDCB1 geometries. According to the values reported in Sect. 2.1, dimensionless T-stresses for the CT and TDCB1 specimens remain relatively low: this promotes collinear propagation of the nucleated cracks with respect to the pre-existing cracks. Crack paths predicted by the PF model for the considered geometries are shown in Fig. 6. They closely reproduce the expected evolution based on T-stress theoretical analysis, in agreement with experimental observations reported in the literature. Propagations remain collinear with the initial pre-cracks, consistently with pure Mode-I loading conditions.

5.2.2. DCB and TDCB2 geometries. As widely discussed in the previous section, CT and TDCB1 geometries are characterized by straight crack paths. In contrast, the remaining specimens under consideration experimentally exhibit curved crack trajectories. The observed behavior is closely related to the magnitude of the dimensionless T-stress τ associated with each geometry. For TDCB2, DCB1, and DCB2, these values are considerably higher than those reported for CT and TDCB1, as highlighted

This preprint has not undergone peer review or any post-submission improvements or corrections. The Version of Record of this article is published in *Zeitschrift für angewandte Mathematik und Physik*, and is available online at https://doi.org/10.1007/s00033-025-02697-2

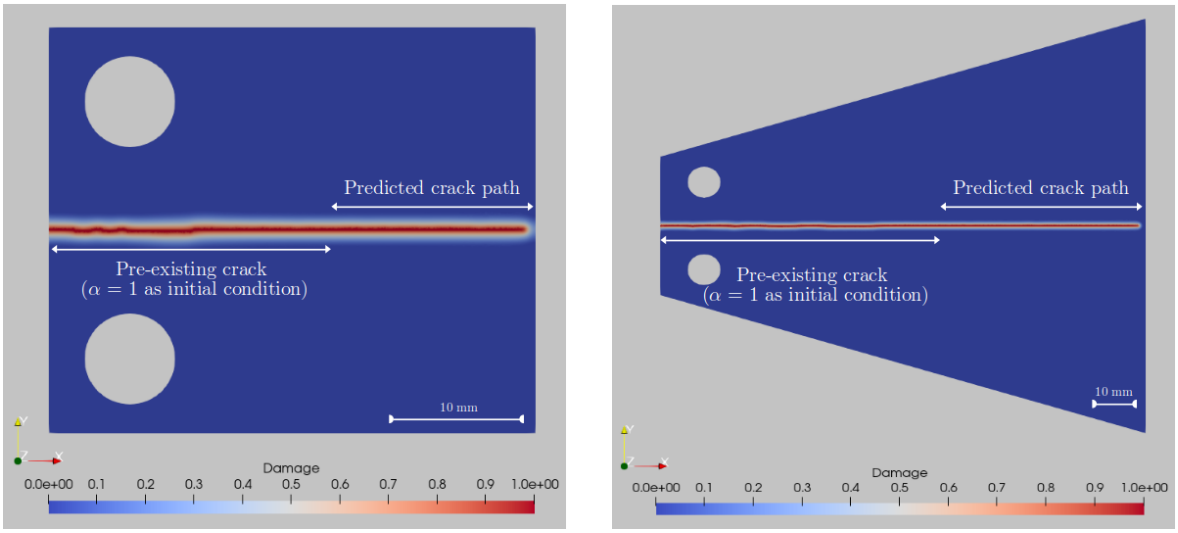

(A) CT specimen (B) TDCB1 specimen

FIGURE 6. Crack paths predicted by the PF model for CT and TDCB1 geometries. Simulations predicted straight crack growth path in full agreement with experimental data [4]

in [4] (see also Table 1). Experimental observations revealed curved crack paths that begin to deviate from pre-cracks shortly after nucleation. It is worth noting that curvatures and the overall shape of the resulting crack paths vary significantly between specimens, highlighting the strong influence of geometric configuration on crack propagation behavior. Fig. 7 shows the crack path predicted by the PF model for the DCB1 geometry: the damage starts to follow immediately a direction that clearly deviates from the original pre-crack alignment. Fig. 8 shows the comparison between the experimental crack paths reported in [4] and PF predictions. Numerical results are displayed as discrete points, each marking the location of a mesh node where the damage variable α exceeds the predefined threshold $\alpha_{\text{tr}} = 0.95$. For all the considered configurations, numerical results accurately catch the specific curvatures of the experimental crack paths, effectively describing their evolution beyond the damage nucleation phase.

Experimental observations show that, in all three geometries featuring a curved crack path, fracture initiation occurs at a non-zero angle. This indicates a sharp deviation of the crack from the pre-crack direction, commonly referred to as kinking [45, 20]. PF simulations eventually describe a non-collinear crack path, but only beyond a certain distance from the initial crack tip.

This preprint has not undergone peer review or any post-submission improvements or corrections. The Version of Record of this article is published in *Zeitschrift für angewandte Mathematik und Physik*, and is available online at https://doi.org/10.1007/s00033-025-02697-2

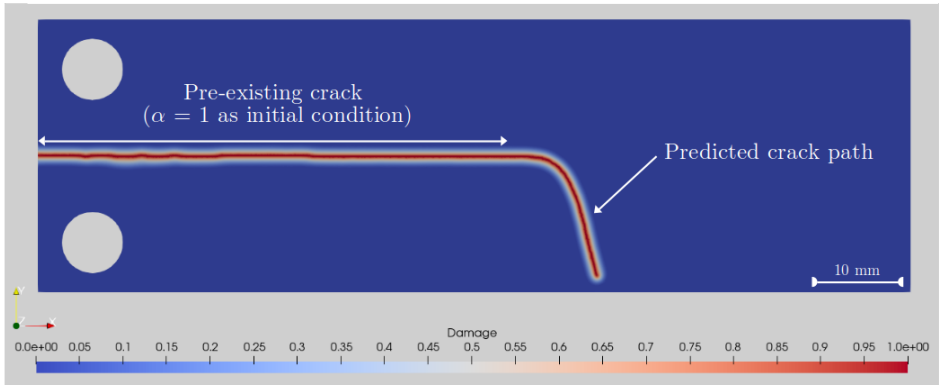

FIGURE 7. Crack path predicted by the PF model for the DCB1 geometry. Simulations predicted a curved growth path in agreement with experimental data [4]

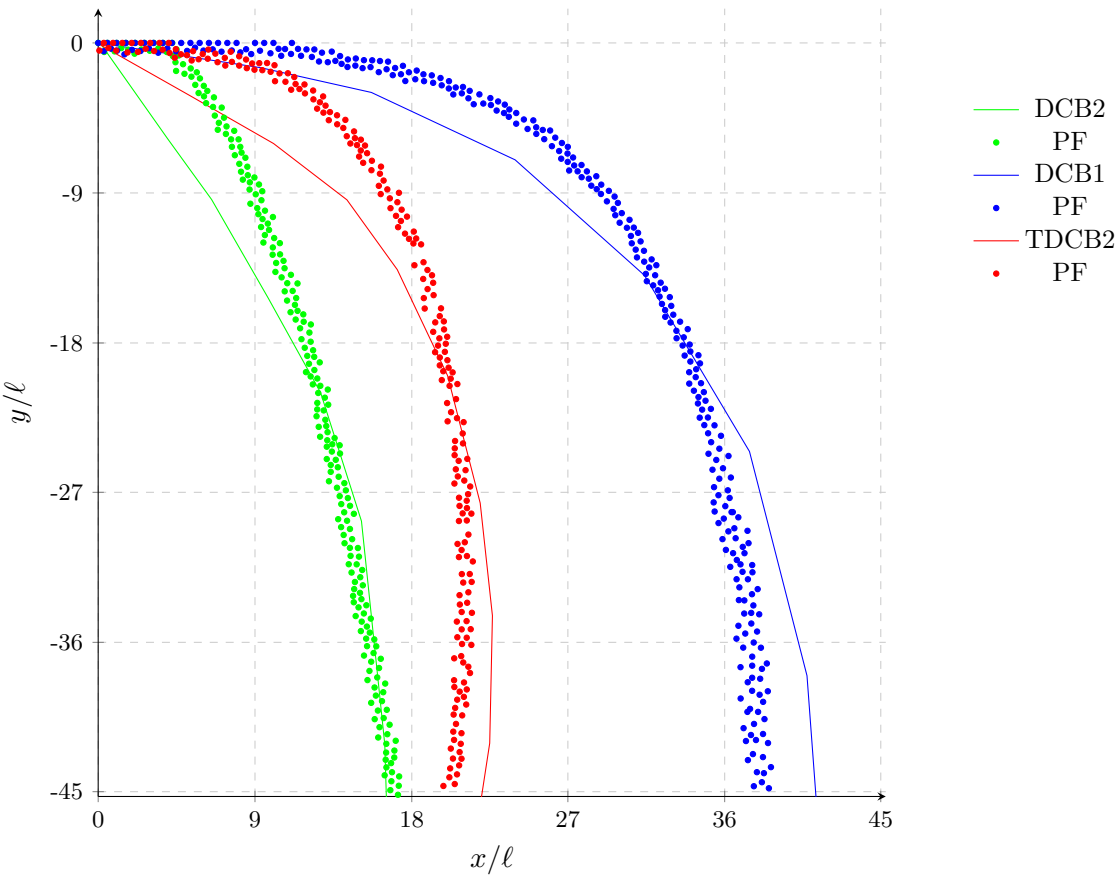

FIGURE 8. Comparison between experimental paths [4] (lines) and PF results (dots) for geometries that exhibit curved crack propagation. (For interpretation of the references to color in this figure legend, the reader is referred to the online version of this article)

This preprint has not undergone peer review or any post-submission improvements or corrections. The Version of Record of this article is published in *Zeitschrift für angewandte Mathematik und Physik*, and is available online at https://doi.org/10.1007/s00033-025-02697-2

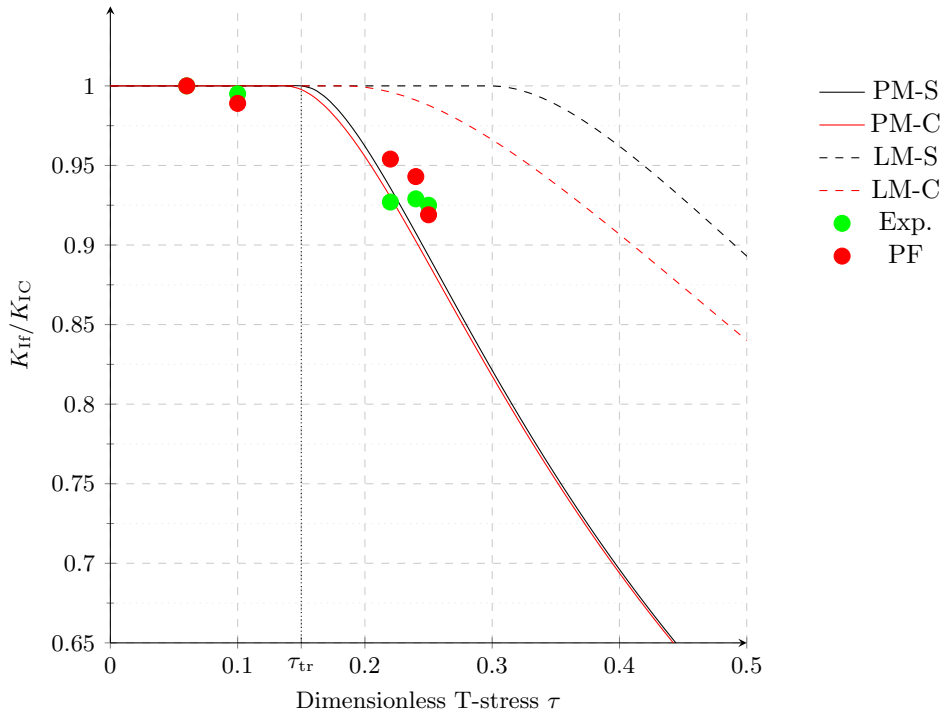

FIGURE 9. T-stress effect on normalized critical SIF K_{If} according to PF simulations (red dots), experimental tests [4] (green dots), PM (continuous lines) and LM (dashed lines). (For interpretation of the references to color in this figure legend, the reader is referred to the online version of this article)

5.3. Comparison with Theory of Critical Distances (TCD) predictions

The following section compares fracture strength predictions from the PM and LM approaches - applied to both straight (PM-S and LM-S) and curved crack paths (PM-C and LM-C) - with PF results and experimental data, and evaluates kinking angles and curvature parameters against experimental observations.

5.3.1. Fracture strength. Fig. 9 presents PF and TCD predictions of the normalized critical SIF K_{If} along with the experimental data reported by Ayatollahi et al. [4] as a function of the dimensionless T-stress τ. PM predictions indicate that, for $\tau > \tau_{tr} = 0.15$, the critical SIF differs from the fracture toughness K_{IC}, suggesting that the behavior is no longer predictable by Linear Elastic Fracture Mechanics. Notably, for the TDCB1 geometry (corresponding to $\tau = 0.1 < \tau_{tr}$), the reference study [4] reports $K_{If}/K_{IC} = 0.995$, indicating that experimentally the critical SIF exhibits a negligible deviation from the fracture toughness. Reported experimental results corroborate PM predictions for both straight and curved crack paths, which exhibit a very similar trend. On the other hand, LM predictions are less accurate than the PM in capturing the transition toward lower fracture strengths. This behaviour aligns with findings from previous studies, which have shown that the PM approach tends to yield conservative estimates of critical loads [38]. Nevertheless, the discrepancy between LM-C predictions and experimental data remains below 8%. A comparison between the results of LM-S and LM-C shows that LM-C starts deviating from the LEFM validity region ($K_{If}/K_{IC} = 1$) at lower τ values. This trend is consistent with the observations reported in [45], where the fracture strength associated with curved crack propagation is found to be lower, or at most equal, to that corresponding to a straight trajectory.

This preprint has not undergone peer review or any post-submission improvements or corrections. The Version of Record of this article is published in *Zeitschrift für angewandte Mathematik und Physik*, and is available online at https://doi.org/10.1007/s00033-025-02697-2

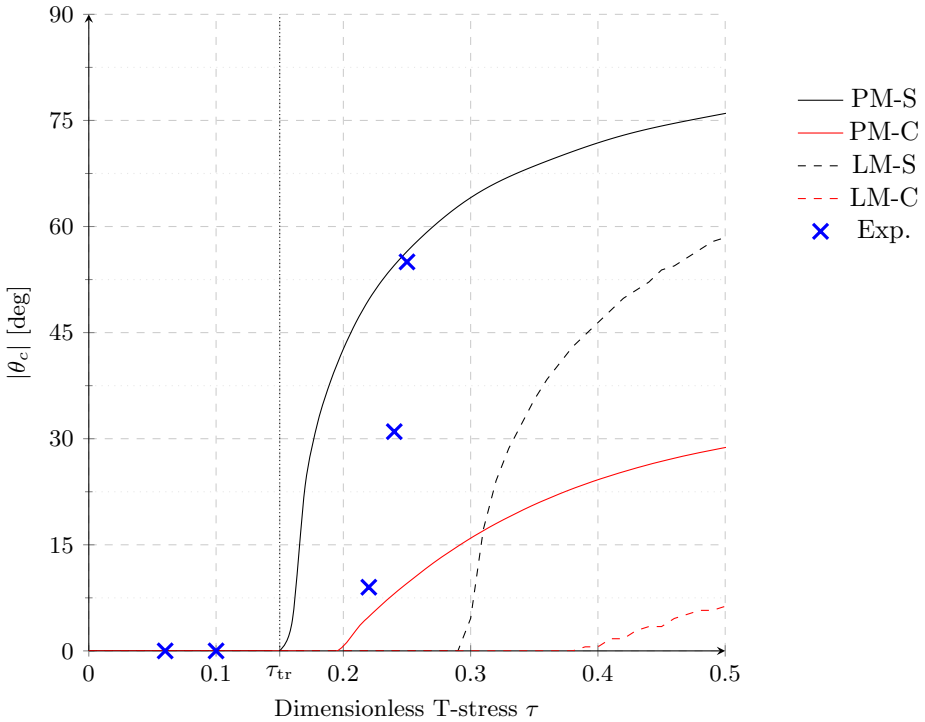

FIGURE 10. Critical kinking angle θ_c according to the experimental tests [4] (blue crosses), PM (continuous lines) and LM (dashed lines) vs. dimensionless T-stress τ. (For interpretation of the references to color in this figure legend, the reader is referred to the online version of this article)

5.3.2. Critical kinking angle. Fig. 10 shows TCD estimations of the critical kinking angle θ_c together with the experimental results provided in [4] as a function of the dimensionless T-stress τ. PM-S captures the transition between LEFM validity range (for $\tau < \tau_{\text{tr}}$) to the onset of crack deviation, accurately reproducing the loss of collinearity in crack propagation once the threshold τ_{tr} is reached. The results are particularly satisfactory, as they closely match the experimental trends as a function of τ. Both PM-C and LM-C predict a deflection for higher values of τ and the magnitude of the predicted kinking angles remain lower than results provided by TCD applied on straight crack advance. This behavior is not surprising, since when predicting the initial propagation direction of cracks using TCD on curved cracks it is also essential to consider predictions of the critical curvature parameter b_c, which are reported in Fig. 11.

5.3.3. Curvature parameter. Fig. 11 depicts TCD predictions of the critical curvature parameter b_c. Plots show that the values of b_c deviate from zero earlier than the kinking angles. This suggests that, according to the models, there exists a range of τ values for which the crack follows a curved path without exhibiting a distinct kink. Fig. 12 compares the initial propagation trajectories predicted by LM-C with the average experimental paths reported in [4]. The comparison highlights that LM-C accurately reproduces the initial shape of the experimental cracks, with slightly lower accuracy for the DCB2 geometry compared to the nearly perfect agreement obtained for TDCB2 and DCB1 geometries. Notably, DCB2 corresponds to the highest value of τ among the tested configurations, and in this case the method still successfully captures the more pronounced deviation of the crack path.

This preprint has not undergone peer review or any post-submission improvements or corrections. The Version of Record of this article is published in *Zeitschrift für angewandte Mathematik und Physik*, and is available online at https://doi.org/10.1007/s00033-025-02697-2

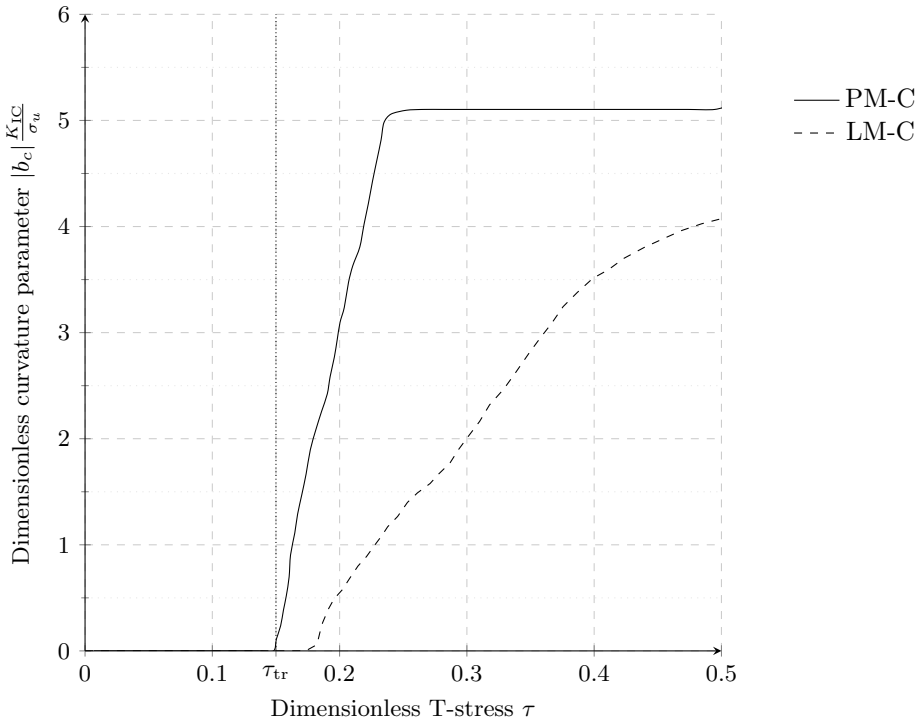

FIGURE 11. T-stress effect on the critical curvature parameter b_c according to the PM (continuous line) and LM (dashed line)

6. Conclusions

This paper presents a computational investigation of critical loads and crack paths in brittle cracked specimens subjected to pure Mode-I loading. PF and TCD models were implemented and validated against experimental results [4], involving five different geometries characterized by different T-stress values. By defining pre-cracks through Dirichlet-type nodal constraints on the damage variable, PF was developed in a quasi-static framework.

The model accurately predicted the average experimental critical loads, with deviations below 10% across all tested geometries. Moreover, the numerical model was proved capable of accurately capturing the distinct crack path curvatures associated with each tested geometry, highlighting the model's sensitivity to the specific features driving crack deviation. Despite the overall satisfactory results, the model exhibited difficulties in accurately capturing the initial crack propagation angles. Future investigations may focus on the implementation of a dynamic PF model, to thoroughly evaluate inertial effects impact on the early post-nucleation crack states.

Finally, PF critical SIFs predictions demonstrate the influence of T-stress on fracture strengths. In addition to match experimental observations, PF numerical outcomes are further supported by predictions from PM and LM, which, as widely discussed in [45], predict a dimensionless T-stress threshold beyond which the structural behavior can no longer be captured by LEFM.

The results of this study highlight that, for applications primarily focused on estimating the fracture strength of cracked components, TCD approaches offer an efficient and robust predictive tool: not only do they deliver accurate strength predictions (in particular the PM), but they also capture the initial crack deviation at the propagation onset. On the other hand, when a full description of the crack path is required, the PF model stands out as the most comprehensive solution, successfully reproducing both straight and curved trajectories, and providing reliable estimates of critical loads and fracture strength across a variety of geometries, all without sacrificing accuracy.

This preprint has not undergone peer review or any post-submission improvements or corrections. The Version of Record of this article is published in *Zeitschrift für angewandte Mathematik und Physik*, and is available online at https://doi.org/10.1007/s00033-025-02697-2

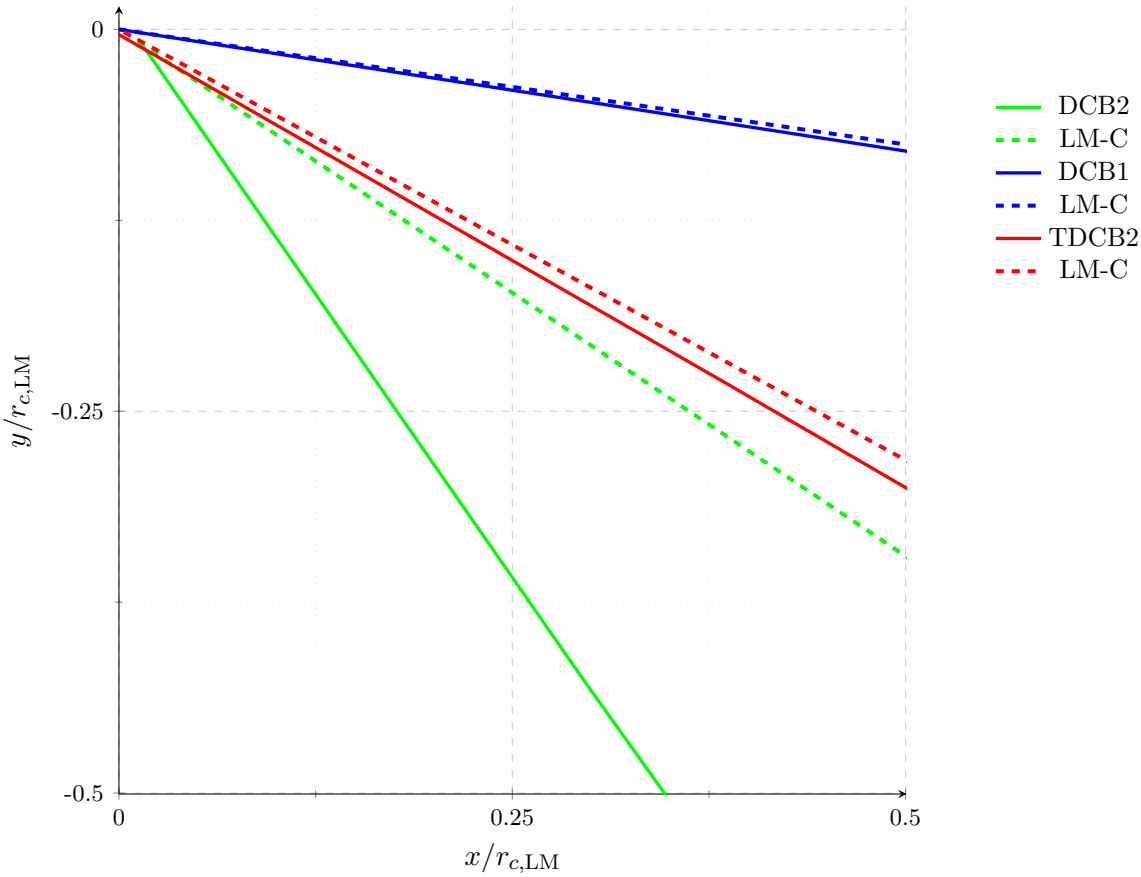

FIGURE 12. Comparison between experimental (continuous lines, from [4]) and predicted crack initiation angles from LM (dashed lines). (For interpretation of the references to color in this figure legend, the reader is referred to the online version of this article)

Competing interests We disclose that, although the author Alfio Grillo is co-editor of ZAMP, he had no involvement in the peer-review process or in the editorial decision-making related to this manuscript.

References

[1] Ambati, M., Kruse, R., De Lorenzis, L.: A phase-field model for ductile fracture at finite strains and its experimental verification. Comp. Mech. **57**, 149–67 (2016)

[2] ASTM E399-20a: Standard Test Method for Linear-Elastic Plane-Strain Fracture Toughness of Metallic Materials. West Conshohocken, PA: ASTM International (2020). DOI https://doi.org/10.1520/E0399-20A

[3] Ayatollahi, M.R., Aliha, M.R.M., Saghafi, H.: An improved semi-circular bend specimen for investigating mixed mode brittle fracture. Engng. Fract. Mech. **78**, 110–23 (2011)

[4] Ayatollahi, M.R., Rashidi Moghaddam, M., Razavi, N., Berto, F.: Geometry effects on fracture trajectory of pmma samples under pure mode-i loading. Engng. Fract. Mech. **163**, 449–61 (2016)

[5] Banichuk, N.V.: Determination of the form of a curvilinear crack by small parameter technique. Izv. An SSSR MTT **7**, 130–7 (1970)

This preprint has not undergone peer review or any post-submission improvements or corrections. The Version of Record of this article is published in *Zeitschrift für angewandte Mathematik und Physik*, and is available online at https://doi.org/10.1007/s00033-025-02697-2

[6] Baratta, I.A., Dean, J.P., Dokken, J.S., Habera, M., Hale, J.S., Richardson, C.N., Rognes, M.E., Scroggs, M.W., Sime, N., Wells, G.N.: DOLFINx: The next generation FEniCS problem solving environment (2023). DOI https://doi.org/10.5281/zenodo.10447666

[7] Becker, T.L., Cannon, R.M., Ritchie, R.O.: Finite crack kinking and t-stresses in functionally graded materials. Int. J. Solids Struct. **38**, 5545–63 (2001)

[8] Bleyer, J.: Numerical tours of Computational Mechanics with FEniCSx (2024). DOI https://doi.org/10.5281/zenodo.10470942

[9] Bleyer, J., Roux-Langlois, C., Molinari, J.F.: Dynamic crack propagation with a variational phase-field model: limiting speed, crack branching and velocity-toughening mechanisms. Int. J. Fract. **204**, 79–100 (2017)

[10] Borden, M.J., Verhoosel, C.V., Scott, M.A., Hughes, T.J., Landis, C.M.: A phase-field description of dynamic brittle fracture. Comput. Methods Appl. Mech. Engng. **217-220**, 77–95 (2012)

[11] Bourdin, B., Francfort, G.A., Marigo, J.J.: Numerical experiments in revisited brittle fracture. J. Mech. Phys. Solids **48**, 797–826 (2000)

[12] Bower, A.F.: Applied mechanics of solids. CRC press (2009). DOI https://doi.org/10.1201/9781439802489

[13] Carpinteri, A., Di Tommaso, A., Viola, E.: Collinear stress effect on the crack branching phenomenon. Mat. Struct. **12**, 439–46 (1979)

[14] Chao, Y.J., Liu, S., Broviak, B.J.: Brittle fracture: variation of fracture toughness with constraint and crack curving under mode i conditions. Exp. Mech. **41**, 232–41 (2001)

[15] Chao Correas, A., Hale, J., Jiménez Alfaro, S., Latyshev, A., Maurini, C.: newfrac/fenicsx-fracture: v1.0 (v1.0) (2024). DOI https://doi.org/10.5281/zenodo.11518791

[16] Chao Correas, A., Reinoso, J., Cornetti, P., Corrado, M.: On the (lack of) representativeness of quasi-static variational fracture models for unstable crack propagation. J. Mech. Physics Solids **186**, 105,573 (2024)

[17] Chao Correas, A., Sapora, A., Reinoso, J., Corrado, M., Cornetti, P.: Coupled versus energetic nonlocal failure criteria: A case study on the crack onset from circular holes under biaxial loadings. Eur. J. Mech. - A/Solids **101**, 105,037 (2023)

[18] Cornetti, P., Pugno, N., Carpinteri, A., Taylor, D.: Finite fracture mechanics: a coupled stress and energy failure criterion. Engng. Fract. Mech. **73**, 2021–33 (2006)

[19] Cornetti, P., Sapora, A., Carpinteri, A.: T-stress effects on crack kinking in finite fracture mechanics. Engng. Fract. Mech. **132**, 169–76 (2014)

[20] Cotterell, B., Rice, J.R.: Slightly curved or kinked cracks. Int. J. Fract. **16**, 155–69 (1980)

[21] De Lorenzis, L., Maurini, C.: Basics of computational methods for fracture (2021). Newfrac Core School notes

[22] De Lorenzis, L., Maurini, C.: Nucleation under multi-axial loading in variational phase-field models of brittle fracture. Int. J. Fract. **237**, 61–81 (2022)

[23] Destuynder, P., Djaoua, M., Lescure, S.: Quelques remarques sur la mécanique de la rupture élastique. J. Mech. Theor. Appl. **2**, 113–35 (1983)

[24] Erdogan, F., Sih, G.C.: On the crack extension in plates under plane loading and transverse shear. J. Basic Engng. **85**, 519–25 (1963)

[25] Geuzaine, C., Remacle, J.F.: Gmsh: A 3-d finite element mesh generator with built-in pre-and post-processing facilities. Int. J. Numerical Methods Engng. **79**, 1309–31 (2009)

[26] Gol'dstein, R.V., Salganik, R.L.: Brittle fracture of solids with arbitrary cracks. Int. J. Fract. **10** (1974)

[27] Heinzmann, J., Carrara, P., Ambati, M., Mirzaei, A.M., De Lorenzis, L.: An adaptive acceleration scheme for phase-field fatigue computations. Comp. Mech. pp. 1–32 (2024)

[28] Infante-Garcia, D., Quinonero-Moya, A., Alvarez-Blanco, M., Giner, E.: Verification of strain energy splits of phase field fracture model using westergaard's problem under mixed-mode loading. Engng. Fract. Mech. **308**, 57–73 (2024)

[29] Jameel, A., Harmain, G.A.: Modeling and numerical simulation of fatigue crack growth in cracked specimens containing material discontinuities. Strength Mat. **48**, 294–307 (2016)

[30] Klinsmann, M., Rosato, D., Kamlah, M., McMeeking, R.M.: An assessment of the phase field formulation for crack growth. Comput. Methods Appl. Mech. Engng. **294**, 313–30 (2015)

This preprint has not undergone peer review or any post-submission improvements or corrections. The Version of Record of this article is published in *Zeitschrift für angewandte Mathematik und Physik*, and is available online at https://doi.org/10.1007/s00033-025-02697-2

[31] Kristensen, P.K., Niordson, C.F., Martínez-Pañeda, E.: An assessment of phase field fracture: crack initiation and growth. Philos. T. Roy. Soc. A **379**, 20210,021 (2021)

[32] Kuhn, C., Noll, T., Müller, R.: On phase field modeling of ductile fracture. GAMM-Mitteilungen **39**, 35–54 (2016)

[33] Leblond, J.B.: Crack paths in plane situations—i. general form of the expansion of the stress intensity factors. Int. J. Solids Struct. **25**, 1311–25 (1989)

[34] Leguillon, D.: Strength or toughness? a criterion for crack onset at a notch. Eur. J. Mech. - A/Solids **21**, 61–72 (2002)

[35] Leguillon, D., Murer, S.: Crack deflection in a biaxial stress state. Int. J. Fract. **150**, 75–90 (2008)

[36] Li, G., Yin, B.B., Zhang, L.W., Liew, K.M.: Modeling microfracture evolution in heterogeneous composites: A coupled cohesive phase-field model. J. Mech. Physics Solids **142**, 103,968 (2020)

[37] Li, T., Marigo, J.J.: Crack tip equation of motion in dynamic gradient damage models. J. Elast. **127**, 25–57 (2017)

[38] Marsavina, L., Sapora, A., Susmel, L., Taylor, D.: The application of the theory of critical distances to nonhomogeneous materials. Fatigue Fract. Engng. Mater. Struct. **46**, 1314–29 (2023)

[39] Molnár, G., Doitrand, A., Estevez, R., Gravouil, A.: Toughness or strength? regularization in phase-field fracture explained by the coupled criterion. Theor. Appl. Fract. Mech. **109**, 102,736 (2020)

[40] Neuber, H.: Theorie der Entlastungskerben, pp. 157–63. Springer (1958). DOI https://doi.org/10.1007/978-3-642-53069-2_7

[41] Nguyen, T.T., Yvonnet, J., Zhu, Q.Z., Bornert, M., Chateau, C.: A phase field method to simulate crack nucleation and propagation in strongly heterogeneous materials from direct imaging of their microstructure. Engng. Fract. Mech. **139**, 18–39 (2015)

[42] Pham, K.B., Hanen, A., Marigo, J.J., Maurini, C.: Gradient damage models and their use to approximate brittle fracture. Int. J. Damage Mech. **48**, 618–52 (2011)

[43] Pham, K.H., Ravi-Chandar, K., Landis, C.M.: Experimental validation of a phase-field model for fracture. Int. J. Fract. **205**, 83–101 (2017)

[44] Rudshaug, J., Børvik, T., Hopperstad, O.S.: Modeling brittle crack propagation for varying critical load levels: a dynamic phase-field approach. Int. J. Fract. **245**, 57–73 (2024)

[45] Sapora, A., Cornetti, P., Mantič, V.: T-stress effects on crack deflection: Straight vs. curved crack advance. Eur. J. Mech. - A/Solids **60**, 52–7 (2016)

[46] Sapora, A., Mantič, V.: Finite fracture mechanics: a deeper investigation on negative t-stress effects. Int. J. Fract. **197**, 111–18 (2016)

[47] Sapora, A., Torabi, A.R., Etesam, S., Cornetti, P.: Finite fracture mechanics crack initiation from a circular hole. Fatigue Fract. Engng. Mater. Struct. **41**, 1627–36 (2018)

[48] Selvarathinam, A.S., Goree, J.G.: T-stress based fracture model for cracks in isotropic materials. Engng. Fract. Mech. **60**, 543–61 (1998)

[49] Seweryn, A.: A non-local stress and strain energy release rate mixed mode fracture initiation and propagation criteria. Engng. Fract. Mech. **59**, 737–60 (1998)

[50] Sims, B., Bird, R.E., Coombs, W.M., Giani, S.: Boundary conditions for pre-existing fractures in phase field fracture models. SSRN (2024)

[51] Smith, D.J., Ayatollahi, M.R., Pavier, M.J.: The role of t-stress in brittle fracture for linear elastic materials under mixed-mode loading. Fatigue Fract. Engng. Mater. Struct. **24**, 137–50 (2001)

[52] Smith, M.: ABAQUS/Standard User's Manual, Version 6.9. Dassault Systèmes Simulia Corp, United States (2009)

[53] Tanaka, K.: Engineering formulae for fatigue strength reduction due to crack-like notches. Int. J. Fract. **22**, 39–45 (1983)

[54] Tanné, E., Li, T., Bourdin, B., Marigo, J.J., Maurini, C.: Crack nucleation in variational phase-field models of brittle fracture. J. Mech. Physics Solids **110**, 80–99 (2018)

[55] Taylor, D.: Geometrical effects in fatigue: a unifying theoretical model. Int. J. Fatigue **21**, 413–20 (1999)

[56] Taylor, D.: The theory of critical distances. Engng. Fract. Mech. **75**, 1696–1705 (2008)

This preprint has not undergone peer review or any post-submission improvements or corrections. The Version of Record of this article is published in *Zeitschrift für angewandte Mathematik und Physik*, and is available online at https://doi.org/10.1007/s00033-025-02697-2

[57] Whitney, J.M., Nuismer, R.J.: Stress fracture criteria for laminated composites containing stress concentrations. J. Compos. Mater. **8**, 253–65 (1974)

[58] Williams, J.G., Ewing, P.D.: Fracture under complex stress—the angled crack problem. Int. J. Fract. Mech. **8**, 441–6 (1972)

[59] Williams, M.L.: Stress singularities resulting from various boundary conditions in angular corners of plates in extension. J. Appl. Mech. **19**, 526–28 (1952)

[60] Wu, J.Y., Nguyen, V.P., Nguyen, C.T., Sutula, D., Sinaie, S., Bordas, S.P.A.: Phase-field modeling of fracture. Advances in Appl. Mech. **53**, 1–183 (2020)

[61] Zhao, Y.H., Xu, B.H.: Effect of t-stress on the mode-i fracture toughness of concrete. Comptes Rendus Mécanique **342**, 490–500 (2014)

Giacomo Petraglia
ORCID: 0009-0002-2630-2907
Politecnico di Torino, Department of Structural, Geotechnical and Building Engineering
Corso Duca degli Abruzzi, 24
10129 Torino
Italy
Corresponding author:
e-mail: giacomo.petraglia@polito.it

Pietro Cornetti
ORCID: 0000-0001-9063-9913
Politecnico di Torino, Department of Structural, Geotechnical and Building Engineering
Corso Duca degli Abruzzi, 24
10129 Torino
Italy

Alfio Grillo
ORCID: 0000-0002-1104-1890
Politecnico di Torino, Department of Mathematical Sciences
Corso Duca degli Abruzzi, 24
10129 Torino
Italy

Alberto Sapora
ORCID: 0000-0003-3181-3381
Politecnico di Torino, Department of Structural, Geotechnical and Building Engineering
Corso Duca degli Abruzzi, 24
10129 Torino
Italy

This preprint has not undergone peer review or any post-submission improvements or corrections. The Version of Record of this article is published in *Zeitschrift für angewandte Mathematik und Physik*, and is available online at https://doi.org/10.1007/s00033-025-02697-2